



ACADEMIC
PRESS

Available online at www.sciencedirect.com

SCIENCE @ DIRECT®

Journal of Solid State Chemistry 172 (2003) 148–159

JOURNAL OF
SOLID STATE
CHEMISTRY

<http://elsevier.com/locate/jssc>

Investigation of the Rb–W–O system in connexion with the superconducting properties of the hexagonal tungsten bronzes

R. Brusetti,^{a,*} P. Bordet,^b and J. Marcus^c

^a Centre de Recherche sur les Très Basses Températures, Centre National de la Recherche Scientifique, BP 166X, 38042 Grenoble Cedex, France

^b Laboratoire de Cristallographie, Centre National de la Recherche Scientifique, BP 166X, 38042 Grenoble Cedex, France

^c Laboratoire d'Etudes des Propriétés Electroniques des Solides, Centre National de la Recherche Scientifique, BP 166X, 38042 Grenoble Cedex, France

Received 5 July 2002; received in revised form 24 November 2002; accepted 19 December 2002

Abstract

The previous studies of the superconducting properties of the hexagonal tungsten bronzes have repeatedly come up against the lack of reproducibility of the data and, at the first place, of the data relating to the stability of superconducting state. We revisited this problem and identified the main causes of these contradictory data in Rb_xWO_3 , among which the major one is the ordering of the alkali atoms. Our study has emerged onto a determination of the x dependence of the order–disorder transition, of the lattice parameters and of the superconducting transition temperature T_c . We have also clarified the crystal structure and examined the mechanisms involved in the oxidation and reduction of this compound. Finally, we have assembled our data to draw a plausible Rb–W–O phase diagram.

© 2003 Elsevier Science (USA). All rights reserved.

Keywords: Order-disorder; transition in Rb_xWO_3 ; Superconductivity; Stability of the superconducting state; Bronzes; Hexagonal tungsten bronzes; Phase Diagram; Rb–W–O

1. Introduction

Much attention has been paid to the ternary metal–tungsten–oxygen system during the last 50 years approximately; among the huge field of phases progressively observed, the alkali metal tungsten bronzes have been probably the best studied. These are non-stoichiometric compounds of general formula $M_x\text{WO}_3$, where M represents an alkali metal and, depending on their structure and electron density, they can form insulators, metals and even superconductors. When the M atoms are small enough (Li, Na, K) their mobility is remarkably high, which has allowed the corresponding bronzes to be considered for promising electrochromic devices and solid electrolytes. Still more recently, the soft chemistry and intercalation techniques have been extensively applied to these bronzes. As for ourselves, we have been interested in the superconducting properties of the hexagonal tungsten bronzes (HTBs) and, more precisely, in Rb_xWO_3 where higher superconduct-

ing transition temperature T_c had been obtained (T_c as high as 7.7 K have been claimed by Sweedler [1]; see also Ref. [18]). Many studies had already been devoted to these bronzes, following extensive investigations on Na_xWO_3 , which is the first oxide where superconductivity has been observed [2], but these studies yielded many conflicting results, and this apparently discouraged further attempts to get a better knowledge of these systems.

We have been encouraged to revisit this issue after superconductivity (and even high-temperature (superficial) superconductivity) was observed in WO_{3-x} [3] and $\text{Na}_{0.05}\text{WO}_3$ [4], respectively. Although we restricted the field of our investigation to the rubidium compound, we shall show that our results can be readily extrapolated to the neighboring compounds.

We have focused a previous paper (we shall refer to as I) [5] on a description of the physical properties of this system. We shall present here complementary results we gathered in the course of our quest for reproducible physical behaviors which are related to the physical chemistry of these compounds. The structure of the HTBs, as described by Magnéli consists of layers of

*Corresponding author.

E-mail address: brusetti@grenoble.cnrs.fr (R. Brusetti).

corner-sharing WO_6 distorted octahedra in the $z = \frac{1}{4}$ and $\frac{3}{4}$ planes of the unit cell (space group $P6_3/mcm$). The M atoms reside in one-dimensional channels parallel to the c -axis in crystallographic sites which are fully occupied when $x = \frac{1}{3}$ (we shall call the stoichiometric content) and three-fourth occupied when $x = \frac{1}{4}$. This structure is stable only if the alkali atoms are large enough (K, Rb, Cs) and if they fill more than a half of the channel sites ($x \geq 0.19$). The space group proposed by Magneli and then by Labbé et al. [6] has been questioned by Sato et al. [7] according to whom it applies only above $T_{c1} \sim 400$ K in Rb_xWO_3 . Below T_{c1} , the exact structure remained unsolved. This is the first question we shall address. Then we shall deal with three main topics:

- the (low-temperature) ordering of the rubidium vacancies, which destabilizes the superconducting state,
- the (high-temperature) reactivity of the HTB in reducing or oxidizing atmospheres, and more generally the stability limits of this phase in the Rb–W–O ternary system,
- the characterization of the acid-etched samples.

2. Experimental

2.1. Samples preparation

As one of the aims of this study was to find the causes of non-reproducible behaviors, we had first to be confident about the composition of our samples. This led us to carry out the major part of this study with powder samples.¹ These have been prepared by the usual solid-state reaction of high-purity powders (W, 99.95% and WO_3 , 99.998%, Alfa Aesar; Rb_2WO_4 , 99.9%; ChemPur) in sealed quartz tubes. The powders were stored in a nitrogen-filled glove box provided with a dehumidification apparatus which achieves a water content less than 2 ppm. They were kept inside this glove box while they were weighted, grinded, thoroughly mixed in an agate mortar and finally introduced in the quartz tubes which were then closed and transferred on the pumping unit. Before the tube was sealed, the mixture was pumped to 10^{-6} Torr and baked repeatedly at about 150°C until we observed no more outgasing. The tube was then heated at 900°C for 2 days. Let us notice that we deliberately limited the reaction temperature to 900°C and took care to minimize the free space left in the reaction tubes for reasons that will appear later (Section 6).

¹This point is discussed in detail in I. Although we have discarded the single crystals in our search for reproducible behaviors, we used them in some particular experiments which are described in I.

The products were analyzed by powder X-ray diffraction patterns collected on a Philips PW-1390 automated diffractometer ($\text{CuK}\alpha_1$ radiation; Si standard). The micro-probe analysis of some of the samples has been achieved on a CAMECA SX 50 EPMA instrument equipped with four WDS and one EDS Tracor spectrometers. Routine analysis has been also done on JEOL JSM-6400 and 840A microscopes.²

2.2. Structure determination of $\text{Rb}_{0.33}\text{WO}_3$

A needle-shape crystal of dimensions $20 \times 20 \times 140 \mu\text{m}^3$ was selected from a well-crystallized powder prepared as described above. The X-ray diffraction data were collected with a Nonius Kappa CCD diffractometer. The $\text{AgK}\alpha$ radiation selected with a graphite monochromator was used. After determination of the crystal orientation matrix and hexagonal unit cell ($a = b \approx 7.39 \text{ \AA}$, $c \approx 7.57 \text{ \AA}$), diffraction data were collected with the rotation technique by measuring 111 frames of 2° oscillation angle and 600 s exposure time per frame. The sample to detector distance was set to 27 mm, and the maximum theta angle was 27.9° , leading to a resolution limit of 0.6 \AA up to which the data collection completeness was 98.5%. Six thousand one hundred and sixty-nine diffracted intensities were extracted with the Denzo-SMN software [8]. The refined cell parameters obtained from the positions of these reflections were $a = 7.3939(1)$ and $b = 7.5758(2)$. The Maxus suite [9] was used for space group analysis and absorption correction using the description of the crystal faces and the Gaussian integration technique [10]. Equivalent reflection averaging and structure refinements were carried out with the Jana2000 program [11].

2.3. Thermochemical measurements

We have searched for enthalpy anomalies associated with structural or order–disorder transitions by using a Perkin–Elmer DSC-7 differential scanning calorimeter, equipped with its Liquid Nitrogen Subambient Accessory, therefore operating under ultrapure helium at ambient pressure. Between 605°C and 950°C , we also performed scanning calorimetry under an ultrapure (5 N) argon flow with a Netzsch DSC 404S apparatus.

We used two methods to study the controlled oxidation or reduction of our powder samples: first we used a thermogravimetric technique, between about 400°C and 500°C , with a Perkin–Elmer TGA 7 analyser. The samples were sieved to retain grain sizes ranging between about 20 and $50 \mu\text{m}$. Isothermal annealings

²The CAMECA SX 50 and JEOL JSM-6400 apparatus are those of the Consortium des Moyens Technologiques Communs, a laboratory of the Institut National Polytechnique de Grenoble.

were performed under high-purity 1 atm oxygen pressure (oxidation) or 0.1 atm pressure of H₂ in Ar.

Heat treatments at higher temperatures, between about 800°C and 950°C and for 10 h, were achieved in a tubular furnace, under a small gas flow of O₂–N₂ mixtures (AIR LIQUIDE, accuracy of mixing 2%).

2.4. Characterization of the superconducting transition

The transition between the normal and superconducting states have been characterized by monitoring the magnetic susceptibility of the powder samples as a function of the temperature. More precisely, the magnetic behavior of a sample (10–100 mg) is deduced from the variation of the mutual inductance between a pair of oppositely wound coaxial pickup coils when the sample is translated from the center of one coil to the other. The major part of the measurements have been done by placing the pickup coils and sample directly in the helium bath of a He⁴ cryostat. The temperature range which can be covered by pumping on the bath or pressurizing it was about 1.1–5 K. When it was necessary to go to higher temperatures, we used another cryostat in which the pickup coils and sample are placed inside a calorimeter. In both cases, the temperature was regulated and measured with an accuracy better than 0.01 K. These cryostats allow to achieve, if necessary, a very fast cooling of the samples down to 4.2 K by lifting them down directly in the helium bath. This is the process we shall call “fast cooling” or “quench.” We used a mutual-inductance bridge which applies only a small ($<2 \times 10^{-4}$ T) low-frequency (33 Hz) magnetic field on the samples, and is able to detect 10⁻⁸ H. A few magnetic susceptibility measurements below 1 K have also been done in a He³–He⁴ dilution refrigerator and, finally, some experiments have been performed in static fields, with a SQUID magnetometer, in which it was possible to control more precisely the annealing of the “quenched” state. As shown and discussed in detail in I, magnetic characterizations of the superconducting transition are better suited than conductivity measurements to the investigations we were concerned with.

3. Results and discussion

3.1. The rubidium concentration domain of the HTB phase

For $0.215 \lesssim x \lesssim 0.33$, the preparation described above yields single-phase samples whose composition can be identified with their nominal composition. This has been confirmed by the micro-probe analysis of some of the samples from which we also estimated the dispersion of the Rb content in our batches at $0.005 \lesssim \delta x \lesssim 0.01$.

For $0.10 \lesssim x \lesssim 0.19$, the X-ray powder diffraction patterns unambiguously display parasitic peaks, which correspond probably to “intergrowth tungsten bronze” (ITB) structures described by Hussain and Kihlberg [12].³ Although no such peaks are usually present in the samples with $0.19 \lesssim x \lesssim 0.215$, we observed indirectly that they contain traces of the neighboring phases. Actually, we have determined the lattice parameters of our samples using a Rietveld analysis and found that they do not depend any more on x below $x_1 \lesssim 0.215 \pm 0.005$ (see I). Consequently, as far as we shall be concerned with samples prepared at high temperatures, we shall consider that nominal rubidium contents lower than the above limiting value cannot represent the true composition of the HTB phase of interest but must be replaced with x_1 . Moreover, each time we shall compare our data to data taken in the literature, we shall correct these similarly. However, we also show in I that x_1 is not the lowest value the Rb content can take in the HTB: lower contents (down to $x \sim 0.19$) can be obtained by means of low-temperature processes, i.e., oxidation at 450°C (see Section 4) or acid etching at room temperature (Section 6).

Since X-rays might not reveal minor structural changes, we checked that the cooling rate between 950°C and room temperature had no influence on the samples properties, except in the above-mentioned $0.19 \lesssim x \lesssim 0.215$ range; we also performed differential thermal analysis in the same temperature range but we found no sign of a phase transition which could explain some conflicting results. This has encouraged us to undertake a new X-ray analysis of this compound and, more precisely, of the stoichiometric compound, in which no complication could arise from the vacancy ordering we shall consider later.

3.2. The crystal structure of Rb_{0.33}WO₃

From previous reports [7], where the $P6_3/mcm$ space group was used, systematic extinction for reflections ($h0l$), $l = 2n + 1$ corresponding to a c glide plane were expected. However, inspection of our data revealed that 178 observed reflections (with $I > 3\sigma(I)$) did not respect these conditions. These reflections could also be clearly observed on diffraction images. The ($00l$), $l = 2n + 1$ extinction condition corresponding to the 6_3 screw axis was respected. In order to compare our data with those of Labbé et al. [7], we first did not consider these reflections and perform a structure refinement using the $P6_3/mcm$ space group. The averaging process yielded

³Such a structure can be described as an ordered intergrowth of slices of HTB with slabs of WO₃ structure type. The lower the M content ($0.06 \lesssim x \lesssim 0.10$) the thinner are the WO₃ slabs. The corresponding X-ray powder diffraction patterns are very complex and are only known for a few K and Cs ITB.

340 unique reflections with $R_{\text{int}} = 6.46\%$. The refinement was carried out on the structure factors of all reflections, using statistical weights and a 2% instability factors. An isotropic extinction correction of type I (gaussian distribution) was applied [13], and all atoms were given anisotropic displacement parameters. The refinements for 19 parameters and 340 observations converged to $R = 3.00\%$, $R_w = 5.64\%$ and $\text{gof} = 2.21$. The results, given in Table 1, are very similar to those reported previously, and the large values of the displacement parameters indicate a noticeable departure from this average structure.

In order to describe these displacements and to explain the presence of the $(h0l)$, $l = 2n + 1$ reflections, we carried out structure refinements in hexagonal subgroups of the $P6_3/mcm$ space group which contain the 6_3 screw axis but not the c glide plane $P6_3$, i.e., $P6_3/m$ and $P6_322$. The $P6_3$ space group gave the best $R_{\text{int}} = 6.02$ and refinement agreement factors with $R = 3.95$, $R_w = 7.35$ and $\text{gof} = 2.25$ for 1133 observations and 23 parameters. The refinements were carried out as described above, but oxygen atoms were given isotropic thermal parameters in order to avoid correlation with local displacements. The resulting structure is shown in Table 1. It is in qualitative agreement with the one reported by Schultz et al. [14] for $\text{K}_{0.33}\text{WO}_3$. However, and as already mentioned by these authors, the intensities of the $(h0l)$, $l = 2n + 1$ reflections is not well described by the model, leading to bad agreement factors for weak reflections. In our case, the R factor for the 128 weakest observed reflections ($|F| < 27$) is 32.0%, while it is 6.8% for the next 128 stronger ($27 < |F| < 48$) and 1.9% for the 128 strongest ($162 < |F| < 463$).

In order to obtain a better description of the superstructure reflections intensities, we lowered the symmetry again by trying the trigonal space group $P\bar{3}1m$, $P\bar{3}$ and $P3$. For these three space groups, the $(00l)$, $l = 2n + 1$ reflections corresponding to the 6_3 screw axis are allowed to exist, and they were introduced in the refinements with 0 intensities. The $P\bar{3}1m$ and $P\bar{3}$ models did not lead to improvements with respect to hexagonal symmetry. However, the $P3$ space group model yielded substantially better agreement factors, with $R_{\text{int}} = 5.47$, $R = 3.66$, $R_w = 5.05$ and $\text{gof} = 1.29$ for 2215 observations and 44 parameters. With this model, the calculated intensities of the $(00l)$, $l = 2n + 1$ reflections were so weak that they could not be detected in our experiment. The weak reflections are also much better described, since the R factors for the three intensity ranges given above are 15.6%, 4.7% and 2.2%, respectively.

The structural parameters and interatomic distances obtained with these three models are given in Tables 1 and 2. It is interesting to note that the average cation–anion distances (1.92 Å for W–O and 3.31 Å for Rb–O) are the same within 0.01 Å. The cation positions are also very close in the three models, the $(h0l)$, $l = 2n + 1$

Table 1
Results of the single-crystal X-ray data refinements for $\text{Rb}_{0.33}\text{WO}_3$

Space group $P6_3/mcm$						
$R_{\text{int}} = 6.44$	$R = 3.0$	$R_w = 5.6$	$\text{gof} = 2.21$	$N = 340$	$N_{\text{par}} = 19$	
Atom	Pos.	x	y	z	U_{iso}	
W	6g	0.48241(8)	0	$\frac{1}{4}$	0.0046(2)	
Rb	2b	0	0	0	0.042(2)	
O1	12j	0.216(1)	0.423(1)	$\frac{1}{4}$	0.014(2)	
O2	6f	0	$\frac{1}{2}$	0	0.017(6)	
Space group $P6_3$						
$R_{\text{int}} = 6.02$	$R = 3.90$	$R_w = 7.3$	$\text{gof} = 2.24$	$N = 1133$	$N_{\text{par}} = 24$	
Atom	Pos.	x	y	z	U_{iso}	
W	6c	0.48240(7)	−0.00018(5)	$\frac{1}{4}$	0.0050(2)	
Rb	2a	0	0	−0.013(3)	0.039(1)	
O1a	6c	0.428(1)	0.218(1)	0.272(1)	0.0046(8)	
O1b	6c	0.210(1)	0.416(1)	0.230(1)	0.005	
O2	6c	0.507(2)	0.021(1)	0.003(2)	0.006(2)	
Space group $P3$						
$R_{\text{int}} = 5.47$	$R = 3.66$	$R_w = 5.05$	$\text{gof} = 1.29$	$N = 2215$	$N_{\text{par}} = 44$	
Atom	Pos.	x	y	z	U_{iso}	
Wa	3d	0.5185(2)	−0.0002(2)	$\frac{3}{4}$	0.0058(2)	
Wb	3d	0.4834(2)	−0.0002(1)	0.24958(6)	0.0038(2)	
Rba	1a	0	0	0.008(2)	0.0358(9)	
Rbb	1a	0	0	0.488(2)	0.045(1)	
O1a	3d	0.591(1)	−0.209(1)	0.7389(9)	0.0091(6)	
O1b	3d	0.800(1)	0.209(1)	0.7385(9)	0.0091	
O1c	3d	0.437(1)	0.216(1)	0.2367(9)	0.0091	
O1d	3d	0.219(1)	−0.215(1)	0.2353(9)	0.0091	
O2a	3d	0.501(2)	0.002(1)	0.986(1)	0.0091	
O2b	3d	0.478(2)	0.479(1)	0.500(1)	0.0091	

For the $P6_3/mcm$ case, the observed reflections which do not respect the c -glide plane have been omitted. N is the number of reflections used in the refinement, N_{par} the number of refined parameters.

reflection intensities being essentially due to small displacements of the oxygen atoms. The model refined in $P6_3$ is quite close to the one reported by Schultz et al. [14] for $\text{K}_{0.3}\text{WO}_3$, and is characterized by the splitting of O1 ($z = \frac{1}{4}$) into two atoms with $z = 0.27$ and 0.23, leading to tilts of the WO_3 octahedra with respect to the basal plane. For the $P3$ model, each of the oxygen position is again split in two (the positions close to $z = \frac{1}{4}$ and $\frac{3}{4}$ are now independent), which gives more degrees of freedom for the anionic arrangement. In this case, the oxygen in the same layers have almost exactly equal z -coordinates, and the tilting found in $P6_3$ no longer exists. On the other hand, the WO_6 octahedra become more distorted, with W–O distances ranging between 1.80 and 2.01 Å. The two descriptions in $P6_3$ and $P3$ lead to different types of anionic displacement schemes. Although our data are in favor of the $P3$ model, it would be important to confirm it with complementary experiments, for example neutron diffraction.

3.3. The order–disorder transition

The ordering of the alkali vacancies in non-stoichiometric HTB has been first observed in Rb_xWO_3 by Sato et al. [7], by neutron-diffraction measurements. Then, Krause et al. [15] have observed similar behaviors in K_xWO_3 by electron diffraction measurements. A quite complex picture emerges from the different ordering schemes which have been proposed. The ordering of the K atoms is the most stable; it occurs above room temperature in the major part of the composition range. On the contrary, the rubidium (long-range) ordering occurs below room temperature and a disordered state can be quenched more easily. It is what we observed, through the cooling-rate dependence of the superconducting transition temperature T_c , in the composition ranges $0.29 \lesssim x \lesssim 0.31$ and $0.19 \lesssim x \lesssim 0.23$.

This cooling-rate effect is exemplified in Fig. 1. One of its unexpected features lies in the fact that the more disordered state displays the higher T_c , contrary to what is observed most commonly. We are not able to observe the cooling-rate effect for $0.23 \lesssim x \lesssim 0.28$ because, as will be described below, the stability of the ordered state increases when x approaches 0.25; then the largest cooling rate we can achieve is not able to prevent the vacancy ordering. We also studied the annealing of the quenched state in three samples with $x=0.19$, 0.22 and 0.29 by following the corresponding shift of the superconducting transition. We observed that the ordering begins above $T_m \approx 110 \pm 10$ K in all samples, which confirms the extreme mobility of the rubidium vacancies.

Taking into account this order–disorder effect allows to describe now an x dependence of the superconducting temperature T_c that seems quite reasonable. This is displayed in the inset of Fig. 1.⁴ Besides the $T_c(x)$ dependence of the slowly cooled and quenched samples, we have also schematized what it should be if any ordering could be prevented. This “no-order” diagram is quite reminiscent of the $T_c(x)$ diagram observed in Cs_xWO_3 (where the ordering of the Cs vacancies is much less easy) and which displays a monotonic increase of T_c with decreasing x . This unusual behavior has also been observed in the tetragonal sodium bronze and its interpretation is discussed in I.

We have characterized more precisely the order–disorder transition by carrying out a calorimetric study of our powder samples between about 350 and 100 K. We observed the enthalpy anomaly accompanying the

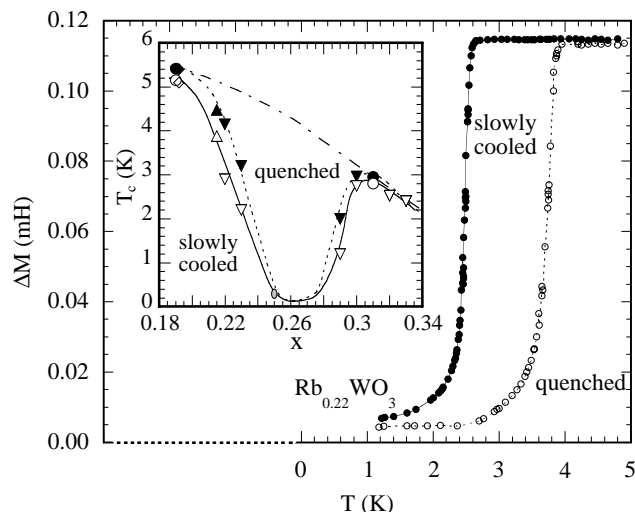


Fig. 1. Superconducting transitions (mutual inductance variations) of a powder sample of $\text{Rb}_{0.22}\text{WO}_3$ after different coolings from ~ 300 K. The inset displays the superconducting transition T_c of the HTB Rb_xWO_3 as a function of the rubidium content x . Empty or full markers refer to measurements after slow cooling or quenching, respectively. The curves are only guides to the eye and the monotonic one extrapolates what we think would be the $T_c(x)$ dependence if the vacancy ordering could be prevented.

order–disorder transformation only in the samples with a rubidium content $x \approx 0.25 \pm 0.01$ (see I). The largest extrapolated peak onset temperature we observed is about 240 K. The corresponding maximum heat absorption is $\Delta H = 80 \pm 10$ J/mol and the maximum entropy increase is $\Delta S = 0.35 \pm 0.05$ J/mol K. A deviation from the optimal composition rapidly shifts down the temperature of the anomaly and, simultaneously, reduces its amplitude. Our results therefore show that the order–disorder transition is first-order only for x in a narrow range around $x=0.25$. Outside this range it should become continuous, since it is still observed in the neutron-diffraction patterns. Actually, in $\text{Rb}_{0.27}\text{WO}_3$, the intensity of the 103/2 superlattice peak continuously decreases to zero on heating up to 200 K [16]. Unfortunately, we have no such information about $\text{Rb}_{0.25}\text{WO}_3$. On the other hand, we have shown in I that the degree of order in $\text{Rb}_{0.25}\text{WO}_3$ is quite low just before it transforms into the high-temperature disordered state. This is in rather good agreement with the simple Bragg–Williams description of an AB_3 alloy, i.e., in this case a $\square\text{Rb}_3$ alloy (where \square stands for “vacancy”) since $\frac{1}{4}$ of the Rb atoms are missing on the rubidium sublattice.

The available data concerning the order–disorder transition temperatures T_{ord} are plotted in Fig. 2. By defining the order–disorder transition temperatures T_{ord} at the onset of the enthalpy anomaly we get a satisfactory agreement with the neutron-diffraction data given by Sato et al. [7]. We have also taken into account the value deduced from electron diffraction experiments on samples with the lowest rubidium content [17].

⁴According to the observations described in Section 1, and as explained in more detail in I, the low $-x$ values ($x < 0.215$) that we plotted in the inset are those of samples processed below 500°C and whose rubidium content has been deduced from a electron probe micro-analysis. The superconducting transition temperature T_c was determined from magnetic measurements because the resistivity data can be misleading (see I).

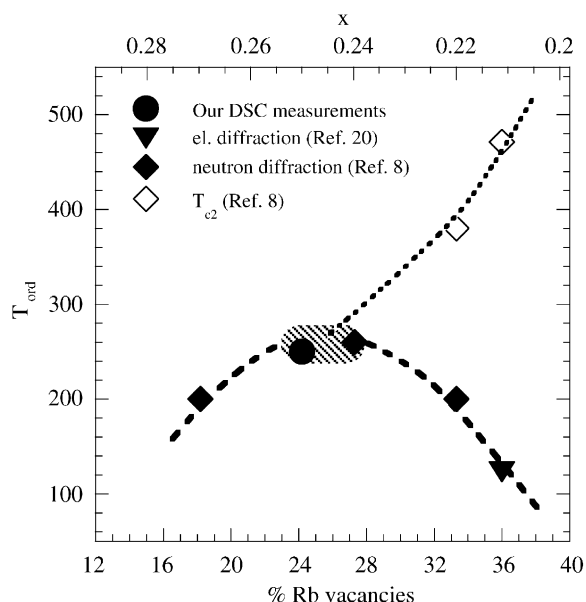


Fig. 2. The x dependence of the order–disorder transition temperature in Rb_xWO_3 . Our DSC measurements show that this transition is first order only in the hatched area around $x=0.25$. The empty diamonds refer to a first stage of the ordering (without expansion in the c direction) observed by Sato et al. [7]: they are displayed here to underline the analogy with the phase diagram proposed by de Fontaine et al. [20] for the cuprates. The curves are only guides to the eye.

Table 2

Principal interatomic distances (Å) for the three structural models given in Table 1

Space group $P6_3/mcm$					
W	O1	1.856(8) × 2	Rb	O1	3.306(6) × 12
		1.98(1) × 2			
	O2	1.898(0) × 2			
Space group $P6_3$					
W	O1a	1.86(1)	Rb	O1a	3.49(1) × 3
		1.975(7)			3.19(1) × 3
	O1b	2.01(1)		O1b	3.24(1) × 3
		1.855(8)			3.30(1) × 3
	O2	1.88(1)			
		1.93(1)			
Space group $P3$					
Wa	O1a	1.87(1)	Rba	O1a	3.32(1)
		2.012(8)			O1b
	O1b	1.878(8)		O1c	3.29(1)
		2.01(1)		O1d	3.27(1)
	O2a	1.80(1)	Rbb	O1a	3.24(1)
	O2b	1.89(1)			O1b
Wb	O1c	1.80(1)		O1c	3.38(1)
		1.993(8)		O1d	3.37(1)
	O1d	1.804(7)			
		2.00(1)			
	O2a	2.00(1)			
	O2b	1.92(1)			

The behavior displayed in Fig. 2 deserves some comments: the narrow composition range in which the transition is first order and the corresponding well-

pronounced maximum in T_{ord} are rather unusual. The occurrence of this maximum, for $\frac{1}{4}$ of the Rb missing on the tunnel sites, probably indicates that the electron system is notably involved. More precisely, we are prone to associate the Rb ordering with a significant reduction of the electron density of states at the Fermi level, D_{FE} . This also implies that ordering of the alkali atoms couple with the host cage, as suggested by some structural studies [7,14]. Consequently, one might reasonably expect that this order–disorder transformation also manifests itself in other physical properties. Actually, it seems to correspond quite well with the anomalies in transport properties which were observed by Stanley et al. [18]. We have investigated this issue but, as is discussed in I, we did not find such a clear correspondence.

Finally, we shall notice that order–disorder phenomena also take place in the high- T_c cuprates [19] (although it is the oxygen vacancies which are involved there) and Fig. 2 is quite reminiscent of the concentration dependence of the ordering temperature as it emerges from the thermodynamical model of de Fontaine et al. [20]. This similitude is still more striking if one takes into account a first stage of the Rb ordering that has been observed by Sato et al. [7] in the low-rubidium-content samples: the corresponding transition temperature T_{c2} increases from about 300 up to ~ 500 K when x decreases from 0.25 down ~ 0.19 , as schematized by the dotted curve in Fig. 2. Let us mention again that these authors also found that a small distortion of the WO_6 cage takes place below about $T_{c1} \sim 400$ K. However, we have not seen any enthalpy anomaly at T_{c1} or T_{c2} , nor have we seen any influence of the cooling rate between 800°C and room temperature.

4. Oxidation of the HTB

Besides the rubidium ordering in the non-stoichiometric Rb_xWO_3 , another cause of the conflicting results mentioned above could lie in accidental oxidations. We observed that the oxidation begins at about 420°C . At temperatures just above this threshold, the mass of the samples seems to increase quite linearly with time. At little higher temperatures, the mass increase follows the approximately parabolic behavior displayed in Fig. 3. The oxidation rate depends on the rubidium content as it appears in the inset, where we plotted the relative mass increase $\Delta m/m$ obtained after a 930 min treatment at 470°C . The relative increase in oxygen content corresponding to the largest $\Delta m/m$ values here observed ($\approx 3 \times 10^{-3}$) is about 1%.

In the $450\text{--}500^\circ\text{C}$ temperature range, the activation energy of the oxidation process is about 1.9 ± 0.3 eV for the slower rate and 1.15 ± 0.15 eV for the faster rate. The X-ray diffraction patterns of the oxidized samples give

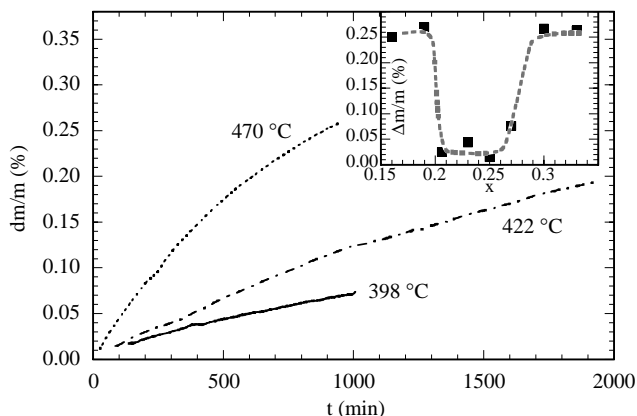


Fig. 3. The time dependence of the relative mass increase of an $\text{Rb}_{0.19}\text{WO}_3$ powder sample under 1 atm O_2 , at different temperatures. The inset shows the x dependence of the relative mass increase after 930 min at 470 °C. The curve is only a guide to the eye. The rubidium content x is here the nominal content.

some insight into the oxidation process. At high rubidium content we identified the oxide in equilibrium with the HTB as a 1:3 polytungstate.⁵ At low rubidium content ($0.26 \gtrsim x \gtrsim 0.19$) the samples contain, instead, what seems to be a 1:6–1:8 polytungstate (see the Appendix).

Since these polytungstates have larger Rb/W ratios than the original HTB, the growing oxide layers must be supplied with rubidium atoms removed from the underlying material. This has been confirmed by the micro-probe analysis of the surface and core of some oxidized samples. It is also confirmed by the corresponding changes in the lattice parameters of the impoverished HTB core. In particular, the values of these parameters in the poorest cores correspond to what is expected for an HTB phase with $0.19 \lesssim x \lesssim 0.20$, extending the linear decrease of c with x observed at higher Rb contents (see Fig. 10 in I). Finally, this Rb transfer is demonstrated quite clearly by the shift of the superconducting transition of this core. This effect is particularly striking in the case of $\text{Rb}_{0.25}\text{WO}_3$, because then an oxidation corresponding to a mass increase $\Delta m/m \approx 2 \times 10^{-3}$ makes superconductivity appear at about 5 K, whereas the original material does not superconduct above 1 K. In samples which have still lower Rb

contents, the Rb supply that is necessary for the growth of the 1:6 polytungstate cannot come from the HTB. Therefore, another phase with $x < 0.19$ should take part in the equilibrium. We have some clues from the diffraction patterns that this third phase is WO_3 , as is to be expected.

We did not find a simple explanation to the behavior displayed in the inset of Fig. 3, i.e., the easier oxidation of the samples whose rubidium contents are at the limits of the composition range. Let us merely mention the various elements which could take part in this behavior:

- The oxidation rate is certainly not limited by the diffusion of the rubidium atoms through the HTB, but could be limited by the diffusion of the oxygen atoms through the oxide layer.
- The migration energy of the oxygen atoms in the 1:3 tungstate is probably lower than in the 1:6's, because the former has a much lower solidification temperature.
- The diffusion rate of these atoms depends on the oxygen activity in the core, which could depend on its rubidium content.
- At the low-rubidium-content limit, a third impoverished material is in equilibrium with the 1:6 tungstate and the HTB phase, probably WO_3 .
- The oxidation rate could be sensitive to the morphology of the crystallites which depends on x .

However that may be, our results show that one should carefully protect these bronzes from accidental oxidations if their rubidium content has to be guaranteed precisely. This also prompted us to estimate the oxygen pressure in equilibrium with the HTB. First, we annealed the powder samples at 900–950 °C in different N_2 – O_2 gas flows and made the following observations:

- oxidation of the low-rubidium-content HTB ($x \approx 0.2$) is complete in O_2 at ambient pressure and yields the 1:6 tungstate plus, possibly, WO_3 .⁶ In a 10^{-3} atm oxygen partial pressure, a noticeable amount of HTB is left. Incidentally, we noticed that the formed oxide reacts with the alumina crucible whereas no reaction is observed with the HTB.
- In a 10^{-4} atm partial pressure, no tungstate is formed but $\text{W}_{18}\text{O}_{49}$ is obtained which forms spectacular bundles of red-purple needles. It coexists with the HTB in which Rb has been concentrated ($x \sim 0.29$).
- In these samples, we also observed weak diffraction peaks that could correspond to other non-stoichiometric WO_{3-y} , like $\text{WO}_{2.9}$, W_5O_{14} , etc. Therefore, when oxygen pressure is between 10^{-3} and 10^{-4} atm, we cannot rule out a possible equilibrium, near

⁵The structures of the rubidium tungstate—and particularly of the 1:3 tungstate—are not well known: the $\text{Rb}_{22}\text{W}_{32}\text{O}_{107}$ formula and the structure proposed by Okada et al. [28] has been questioned by other authors; this uncertainty appears clearly by comparing the intensities and, to a lesser extent, the positions of the diffraction peaks given in the literature. Probably, the composition and structure of these oxides noticeably depends on the elaboration process, due to the extreme adaptability of the WO_6 octaetra which favor the formation of pseudo-phases. We encounter the same problem dealing with the WO_{3-y} compounds. This contributes to make the identification of the parasite peaks in the diffraction patterns much troublesome.

⁶As described in the appendix, we cannot easily distinguish the X-ray signature of small amounts of WO_3 when it coexists with a 1:6–1:8 tungstate.

900°C, between these low- x Rb_xWO_3 and various WO_{3-y} ($0 \lesssim y \lesssim 0.38$). We did not try to clarify this point because it seemed a rather desperate enterprise. Actually, about 15 WO_{3-y} formulas have been already identified in this y range and others could probably be found, in view of the extreme adaptability of the WO_6 octahedras.

- In this temperature range and in oxygen partial pressures above $\sim 10^{-3}$ atm, oxidation of the nearly stoichiometric HTB also yields the 1:6 tungstate. In a 10^{-4} atm partial pressure no oxidation is observed; on the contrary, the HTB crystallites display more regular natural faces as if recrystallization had occurred.
- This implies that the oxygen pressure in equilibrium with the HTB at 900–950°C should be about 10^{-3} – 10^{-4} atm. It is probably higher when the rubidium content is lower and, as can be expected from the usual behavior of oxides, it decreases with temperature, as indicated, for instance, by the oxidation of the stoichiometric samples in 10^{-4} atm O_2 , if they are cooled too slowly from 950°C.

These results prompted us to complete our investigation by looking more systematically for the phases which can be in equilibrium with the HTB in the Rb–W–O system.

5. Reduction of the HTB

First we checked that the oxidation process occurring in the 450–500°C range and described above was reversible. We annealed our powder samples in the TGA analyser under a 0.1 atm pressure of H_2 in Ar. We observed a reduction rate of about the same order than the oxidation rate. By reducing the previously oxidized samples we can remove the oxide phase before we produce reduced phases. We noticed that the lost mass was greater when the samples had already suffered previous reduction(s), but this could follow from a decrease of the residual H_2O pressure in the balance enclosure. In contrast to the profound effect of the oxidations, we observed that oxygen losses greater than 3% seem to hardly alter the HTB phase: the superconducting transition is little changed and the lattice parameters are not significantly modified. Since this suggests that the oxygen content of this phase has not been reduced, we should have in these reduced samples another phase of low oxygen content.

In order to understand the reduction mechanisms involved in these TGA experiments we tried to prepare materials with O/W ratios much smaller than 3, i.e., RbW_3O_7 and $\text{RbW}_5\text{O}_{11}$ (corresponding to $\text{RbO}-3\text{WO}_2$ and $\text{RbO}-5\text{WO}_2$, respectively). The appropriate mixtures of W, WO_3 and Rb_2WO_4 have been allowed to

react 24 h at 900°C in sealed quartz tubes before we quenched them in water. In both cases the main reaction product is the HTB and, more precisely the stoichiometric $\text{Rb}_{0.33}\text{WO}_3$ with its characteristic superconducting transition ($T_c = 2.2 \text{ K} \pm 0.1 \text{ K}$) which does not depend on the low-temperature cooling rate; the corresponding lattice parameters also agree with this Rb content. In each mixture, the HTB coexists with tungsten and an oxide phase: in the $\text{RbO}-5\text{WO}_2$ mixture we find the diffraction peaks corresponding to WO_2 , whereas in $\text{RbO}-3\text{WO}_2$ they correspond to the 1:2 tungstate $\text{Rb}_2\text{W}_2\text{O}_7$ [21], which explains the effective sintering observed in this mixture since this tungstate has the lowest melting temperature (about 700°C).

These results explain the behavior of the Rb_xWO_3 samples which have been moderately reduced in the TGA experiments described above:

- reduction consumes the stoichiometric HTB without affecting its composition in the residue;
- reduction of the rubidium-poor HTB produces only slightly enriched residues because they are in equilibrium with extremely reduced phases: for instance, reducing by 3% the oxygen content of an $\text{Rb}_{0.20}\text{WO}_3$ sample can be achieved by converting 90% of the initial HTB in $\text{Rb}_{0.222}\text{WO}_3$ and 10% in WO_2 . If the same reduction also produces W, the enrichment of the remaining HTB will be still lower.

6. Stability of the HTB

Small samples were also annealed in sealed quartz tubes which had been evacuated down to 10^{-5} Torr, in order to reproduce a common homogenization technique. We used different annealing temperatures T_a between 850°C and 950°C and different cooling rates. Two kinds of behaviors have been observed after quenching the samples from T_a , depending on the Rb content of the samples:

- In low-rubidium-content HTB ($x \lesssim 0.25$), we quite systematically observe that the free surfaces of the samples are bristling with $\text{W}_{18}\text{O}_{49}$ needles with different abundances. Similar needles are also found on the quartz wall or on minute isolated grains stuck on it, indicating that these HTB are probably in equilibrium with a noticeable pressure of WO_3 vapor which can condense on some defects. The microprobe analysis of some of these vapor-grown crystals confirms they are free from rubidium.

This could explain some contradictory data on the x dependence of the physical properties near the low- x limit of the HTB composition range. Actually, these annealings in static vacuum result in a rubidium enrichment of the remaining HTB with a

corresponding reduction of its T_c . At the same time, oxygen should have been transferred from WO_3 to a low-rubidium-content tungstate. Although there is no clear evidence of a third phase in the X-ray spectra of these samples, we infer that a 1:8 polytungstate could be present. This is supported by the analogy with the K–W–O system in which the 1:6 and 1:8 oxides have hexagonal structures and X-ray patterns very similar to the HTB's (see Ref. [22]) and can form a solid solution (see the appendix) and therefore small amounts of such an oxide could easily go unnoticed.

- After the same treatment, at $T_a \gtrsim 900^\circ\text{C}$, on nearly stoichiometric rubidium HTB, we observe that the quartz wall is frosted in the neighborhood of the sample. This is the signature of a reaction with the alkali atoms. The SEM examination of the quartz wall shows it has superficially crystallized but no rubidium is detected in the disturbed layer, as if these atoms had only catalyzed the SiO_2 crystallization. Moreover, weak parasitic peaks are found in the X-ray spectra of the quenched samples and these peaks seem to correspond to the 1:3 tungstate. We first suspected that the rubidium had partly reduced SiO_2 and released enough oxygen to oxidize the HTB but, beside the fact that this seems contrary to the thermochemical data, this could not explain why no parasitic phase is found in the slowly cooled samples. We think the behavior of these samples is more probably related to their partial decomposition, involving a sensible pressure of rubidium: we speculate that the outer part of each grain disproportionates, giving an impoverished layer of HTB (i.e., with $x < 0.33$) plus a rubidium tungstate with a composition corresponding to the 1:3 tungstate, therefore in the liquid state at T_a . Actually, after these treatments we have often observed that some kind of melting had occurred, giving grains with rounded seemingly vitrified faces.

The different decomposition processes occurring in these bronzes, depending on their rubidium content, is reminiscent of the vaporization of the potassium tungsten bronzes: according to Clark and Mart [23], the hexagonal $\text{K}_{0.22}\text{WO}_3$ yields a $\text{W}_{18}\text{O}_{49}$ residue, whereas the tetragonal $\text{K}_{0.43}\text{WO}_3$ yields the 1:2 tungstate $\text{K}_2\text{W}_2\text{O}_7$.

More complex situations can also occur: by preparing an $\text{Rb}_{0.26}\text{WO}_3$ sample according to the procedure proposed by Stanley et al. [18] (a solid-state reaction at 950°C for 5 days) we obtained, in addition to the usual partly sintered powder, a few milligram of needle-like crystals. These often radiate in bundles from tiny crystals attached to the quartz surface, which shows that they grew from the vapor. Most of these needles are

dark blue and display the hexagonal symmetry of the HTB; their length can be about 5 mm along the c -axis. We also observed light-blue whiskers and even transparent ones, some curved and even curled whiskers. As the quartz tube has also been attacked during this treatment we think that noticeable partial pressures of Rb, WO_3 and WO_2 have been produced and have allowed the growth of the needle-like crystals and whiskers in non-equilibrium processes. Some of these are probably WO_{3-y} or polytungstate crystals but the needles could also result from the intergrowth of the HTB phase with these insulating phases: this is suggested by their very peculiar electrical transport properties, as described in I, and also by the close similarity between the HTB, the 1:6 polytungstate [22], and the $\text{W}_{18}\text{O}_{49}$ structures [23].

7. Acid-etching

It was known for a long time that acid etching could remove the Rb ions from the HTB and considerably enhance T_c [24]. However some authors have interpreted this enhancement as a surface effect [25]. We have investigated this effect a little further because we noticed that the acid-etched samples could have a higher T_c than any sample prepared at high temperature. As already discussed in Section 1, we think this is due to the fact that the removal of the Rb at low temperature preserves the HTB structure down to $x \sim 0.19$, whereas this is not stable below $x \sim 0.21$ at $\sim 950^\circ\text{C}$. We have shown in Section 4 that oxidations at moderate temperatures ($\sim 450^\circ\text{C}$) have a similar effect on the HTB cores under the oxide layer.

Concentrated HCl was used at 295 and 310 K, for periods ranging from a day up to a few months. The rubidium contents of the etched samples were deduced from their T_c and lattice parameters. In ambiguous cases, micro-probe analyses were also performed. The homogeneity of these samples could be estimated from the width of their superconducting transition and their diffraction peaks.

We have first etched stoichiometric electrocrystallized crystals weighing 10–20 mg and observed quite unpredictable reaction rates: some crystals were not modified at all, whereas others had reached the lowest Rb concentration ($x \sim 0.19$) after the same time, as if the surface of some crystals were quite inert. We obtained more reproducible reactions by using powdered samples, but then the impoverished powders were rather inhomogeneous. We also checked that the removal of the rubidium atoms could just as well be achieved starting from a powder with $x = 0.22$ or 0.26 as starting from $x = 0.33$. Finally, we observed that, after a long time rest, a white-yellow precipitate could appear in the solution; the X-ray analysis of the powders obtained

after filtration and evaporation showed the solution contained RbCl, whereas the precipitate yielded a WO_3 hydrate⁷.

These reaction products are rather puzzling since they seem to imply a cationic exchange at the surface of the crystals that should consume the external HTB layers without affecting the composition of the bulk. On the contrary it is clear that the rubidium atoms are driven toward the surface during the reaction, which implies complex chemical mechanisms at the solid–liquid interface. For instance, we could imagine that an hydronium tungstate and RbCl can be formed at the interface between the HTB and the HCl solution, provided rubidium ions can be drawn out from the underlying lattice.

The poor homogeneity of the etched HTB powdered samples is also difficult to explain since it does not seem to be improved by prolonging the treatment beyond the first days. We think it could have several causes: (i) passivation probably affects differently each crystallite, depending on the crystallographic orientation and oxidation state of the crystal faces; for instance, the removal of the rubidium atoms could be very slow in those crystals where it only proceeds through small spots on the surface; (ii) the force driving this removal should decrease with the Rb content in the bulk and vanish when $x \sim 0.19$, corresponding to the stability limit of the HTB. Actually no WO_3 or ITB are found in the powder samples after etching. (iii) extended internal defects, like grain walls or intercalated WO_3 planes similar to those found in the ITB, could prevent the Rb transfer from the bulk to the surface. Therefore, the etching reaction could be still incomplete after several weeks at room temperature.

8. The Rb–W–O phase diagram

The observations we have described above allow to complete the phase diagram of the condensed Rb–W–O system. This is displayed in Fig. 4 in which we have chosen Rb_2O , WO_3 and W as components and restricted our field to the most interesting part, bounded by Rb_2WO_4 (the 1:1 polytungstate), WO_3 , and the $\text{W} \cdot \text{WO}_3$ mixture (what would be W_2O_3). This is merely a schematic tentative view and very extensive work would be necessary to get a better picture of this complex system, i.e., to determine the temperature dependence of the various equilibria, the corresponding oxygen partial pressures, and also of the Rb, WO_3 and, perhaps, WO_2 pressures.

Besides the volatility of these species, a major cause of complexity lies in the fact that the HTB and ITB phases, the WO_{3-y} field and probably the 1:6–1:8 polytungstate

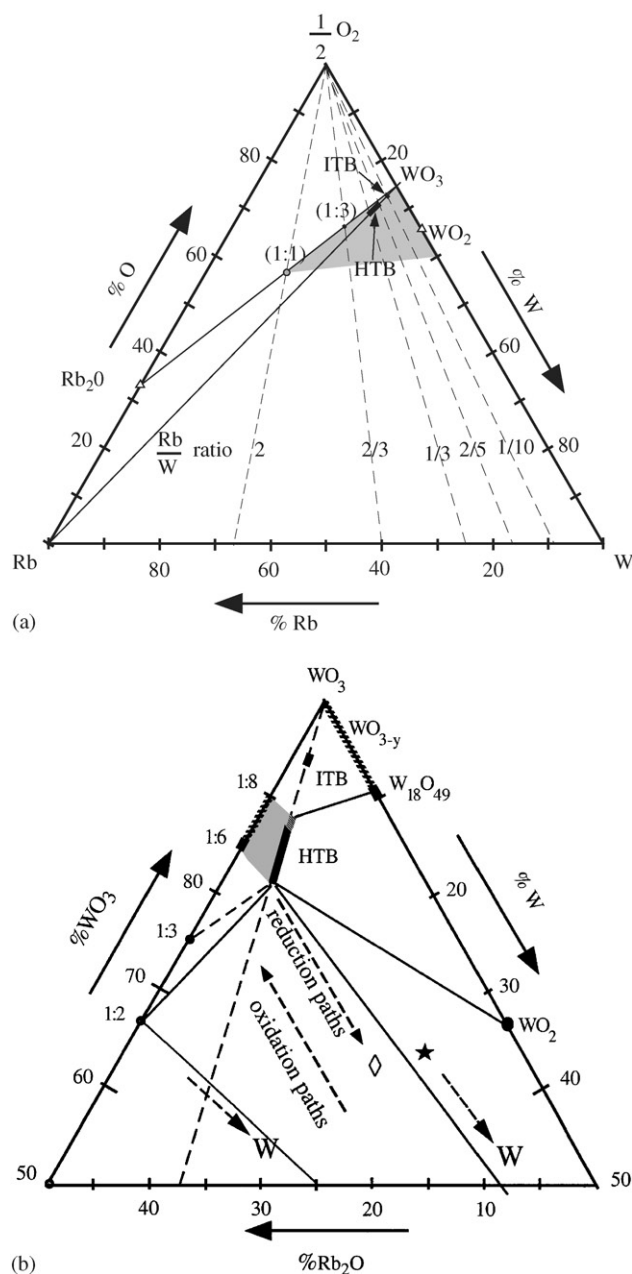


Fig. 4. (a) An overview of the Rb–W–O phase diagram from which is extracted, in (b), the Rb_2O – W_3O –W triangle that involves the rubidium tungsten bronzes. The phase relations are given for temperatures of about 900°C , except when indicated by dashed lines (for more details see Sections 4 and 5). The shaded area represents the plausible connections between the non-stoichiometric HTB and the probable 1:6–1:8 solid solution (see appendix). The diamond and the star indicate what would be the representative points of RbW_3O_7 and $\text{RbW}_5\text{O}_{11}$, respectively. (see Section 5).

domain behave as solid solutions or pseudo-phases. We schematized this aspect in our ternary diagram where we have shown, moreover, that the ITB is probably not stable below about 800°C , like the corresponding potassium bronze [26].

⁷Curiously, the diffraction peaks observed agree with those given for a quite rare $\text{WO}_3\text{H}_2\text{O}$ mineral (JCPDS files 43-679 and 84-886).

It should be remembered also that the low-rubidium-content boundary of the HTB phase shifts from $x \sim 0.19$ below 500°C up to $x \sim 0.21$ at 950°C (Section 1). Finally, the oxidation of $\text{Rb}_{0.33}\text{WO}_3$ deserves special attention: at low temperature ($420\text{--}500^\circ\text{C}$) and under 1 atm O_2 it yields the 1:3 tungstate, in equilibrium with an impoverished HTB (with $0.33 \gtrsim x \gtrsim 0.28$), whereas a 1:6–1:8 polytungstate is produced at higher temperatures ($900\text{--}950^\circ\text{C}$). However, at these temperatures we find again the 1:3 tungstate when $\text{Rb}_{0.33}\text{WO}_3$ decomposes under low pressure (Section 6).

On the contrary, when $0.28 \gtrsim x \gtrsim 0.19$, oxidations under 1 atm O_2 always yield a 1:6–1:8 polytungstate, whereas $\text{W}_{18}\text{O}_{49}$ is produced at low pressures.

9. Conclusion

We have identified the main reasons why the available results on the physical properties of the HTB were so contradictory. Among these reasons the most important is the low-temperature ordering of the rubidium vacancies that destabilizes the superconducting state, probably by inducing simultaneously a strong reduction of the electron–phonon coupling and of the electron density of state at the Fermi level (see I). We have shown that the order–disorder transition is first order only when one quarter of the rubidium atoms are missing; the ordering is then the most stable and, as it cannot be quenched, it has the most profound effect on the electron properties. We have shown also that misleading results could be obtained on vapor-transported samples. This prompted us to study more systematically the effect of oxidizing or reducing atmospheres, as well as the stability of the HTB in vacuum, at high temperature. By assembling all our data we have been able to complete significantly our knowledge of the ternary Rb–W–O system and to draw a coherent picture of the behavior of Rb_xWO_3 and of its superconducting state. Moreover, it appears now that the broad lines of this picture can also be applied to other non-stoichiometric tungsten bronzes, which gives more weight to the unusual behavior they share, when we can get rid of the M vacancy ordering, i.e., the increase of the superconducting temperature T_c with the decrease of the electron density of states.

Many physico-chemical properties of the $M_x\text{WO}_3$ bronzes would deserve further experimental and theoretical investigations: particularly, the mechanisms involved in their oxidation/reduction and the thermodynamics of the M atom ordering. Let us stress, finally, that these superconductors are close neighbors of the tungsten oxides, tungstate and polytungstates in which one can find insulating or polaronic, piezoelectric or ferroelectric behaviors. Considering the remarkable structural compatibility of these systems, this seems to

offer a good opportunity to realize interesting electronic devices.

Acknowledgments

We are grateful to Y. Monfort for communication of unpublished data. We are thankful to Prof. P. Touzain (LEPMI / ENSEEG) for his contribution to the analysis of the etching reaction products. We are indebted to X. Chaud for his technical support in the oxidation experiments, to P. Amiot and A. Hadj-Azzem for the X-ray powder diffraction measurements and SEM examinations and analysis. We greatly acknowledge stimulating discussions with C. Chatillon (LTPCM/ENSEEG) and O. Bethoux.

Appendix

Probably, like in the K–W–O system, Rb_2O and WO_3 can mix continuously in the 1:6–1:8 range, giving a pseudo-phase with only slightly composition-dependent diffraction patterns [22]. As far as the 1:6 rubidium tungstate is concerned, the two diffraction patterns that have been described also differ slightly [21, 27]. Our observations sometimes better agree with one or the other description. To clarify this point we have prepared a 1:8 mixture, first in a sealed evacuated quartz tube, which has been quenched in water after a 24 h treatment at 950°C . In this sample, we observed rather well-developed transparent crystals of various colors and shapes, mostly on its free surface. Then the same sample has been grinded, compressed in a platelet, annealed for 24 h at 950°C in an alumina crucible at ambient atmosphere and cooled in a few minutes down to less than 400°C . In this case, no crystals of macroscopic size were obtained; the platelet, which had only small contact areas with the walls of the alumina boat and no contact with its bottom, was pale blue-green. Below the platelet, the bottom of the alumina boat was covered with a light-yellow layer. The diffraction patterns of all these substances was similar and most of the reflections were compatible with those described in Ref. [21] or [27]. Weak supplementary reflections were also present, the stronger being often observed in the spectra of the oxidized HTB samples. In other respects, we cannot guarantee that no WO_3 was left in our 1:8 mixture after these treatments since the main reflections of WO_3 coincide with reflections that can be attributed to the polytungstate. Finally, after the annealing of the sample at 950°C in air, we observed a loss of mass of about 20% that could be attributed to a sublimation of WO_3 . Obviously, understanding the equilibriums involved in the 1:6–1:8 region of the polytungstate phase diagram would imply a substantial amount of work. However we

think that probably, under some conditions (low oxygen pressure and confinement), the Rb–W–O system can yield the same kind of pseudo-phase in the 1:6–1:8 region as its K equivalent.

References

- [1] A.R. Sweedler, Ph.D. Thesis, University of California, San Diego, 1969, unpublished.
- [2] Ch.J. Raub, A.R. Sweedler, M.A. Jensen, S. Broadston, B.T. Matthias, *Phys. Rev. Lett.* 13 (1964) 746.
- [3] A. Aird, E.K.H. Salje, *J. Phys.* 10 (1998) L377, L569.
- [4] S. Reich, Y. Tsabba, *Eur. Phys. J. B9* (1999) 1; Y. Levy, O. Millo, A. Sharoni, Y. Tsabba, G. Leituss, S. Reich, *Europhys. Lett.* 51 (2000) 564.
- [5] R. Brusetti, P. Haen, J. Marcus, *Phys. Rev. B* 65 (2002) 144528.
- [6] P. Labbé, M. Goreaud, B. Raveau, J.C. Monier, *Acta. Crystallogr. B* 34 (1978) 1433.
- [7] M. Sato, B.H. Grier, H. Fujishita, S. Hoshino, A.R. Moodenbaugh, *J. Phys. C* 16 (1983) 5217.
- [8] Z. Otwinowski, W. Minor, In: C.W. Carter Jr., R.M. Sweet (Eds.), *Methods in Enzymology*, Vol. 276, Academic Press, New York, 1997, pp. 307–326.
- [9] S. Mackay, C.J. Gilmore, C. Edwards, N. Stewart, K. Shankland, *MaXus Computer Program for the Solution and Refinement of Crystal Structures*, Bruker Nonius, The Netherlands, MacScience, Japan & The University of Glasgow, 1999.
- [10] P. Coppens, in: F.R. Ahmed, S.R. Hall, C.P. Huber (Eds.), *Crystallographic Computing*, Munksgaard, Copenhagen, 1970, pp. 255–270.
- [11] V. Petricek, M. Dusek, *Jana2000*, Institute of Physics, Academy of Sciences of the Czech Republic, 2000.
- [12] A. Hussain, L. Kihlborg, *Acta. Crystallogr. A* 32 (1976) 531.
- [13] J. Becker, P. Coppens, *Acta Crystallogr. A* 30 (1974) 129.
- [14] A.J. Schultz, H. Horiuchi, H.B. Krause, *Acta Crystallogr. C* 342 (1986) 641.
- [15] H.B. Krause, R. Vincent, J.W. Steeds, *Solid State Commun.* 68 (1988) 937.
- [16] M. Sato, B.H. Grier, G. Shirane, H. Fujishita, *Phys. Rev. B* 25 (1982) 501.
- [17] Y. Monfort, P. Labbé, M. Goreaud, G. Allais, 1982, unpublished.
- [18] R.K. Stanley, R.C. Morris, W.G. Moulton, *Phys. Rev. B* 20 (1979) 1903.
- [19] B.W. Veal, H. You, A.P. Paulikas, H. Shi, Y. Fang, J.W. Downey, *Phys. Rev. B* 42 (1990) 4770.
- [20] D. de Fontaine, G. Ceder, M. Asta, *J. Less-Common Met.* 164 & 165 (1990) 108.
- [21] L.L.Y. Chang, S. Sachdev, *J. Am. Ceram. Soc.* 58 (1975) 267.
- [22] P. Goodman, *Acta Crystallogr. B* 32 (1976) 3280; A. Klug, *Mater. Res. Bull.* 12 (1977) 837; A. Hussain, L. Kihlborg, A. Klug, *J. Solid State Chem.* 25 (1978) 189.
- [23] N.J. Clark, P.L. Mart, *Mater. Res. Bull.* 18 (1983) 951.
- [24] J.P. Remeika, T.H. Geballe, B.T. Matthias, A.S. Cooper, G.W. Hull, E.M. Kelly, *Phys. Lett.* 24A (1967) 565; C.N. King, J.A. Benda, R.L. Greene, T.H. Geballe, In: R.H. Kropschot, K. D. Timmerhaus (Eds.), *Proceedings of the 13 International Conference on Low Temperature Physics*, Boulder, CO, 1972, University of Colorado Press, Boulder, CO, 1973.
- [25] A.J. Bevelo, H.R. Shanks, P.H. Slides, G.C. Danielson, *Phys. Rev. B* 9 (1974) 3220; I. Lefkowitz, *Ferroelectrics* 16 (1977) 239.
- [26] L. Kihlborg, in: R. Metselaar, H.J.M. Heijligers, J. Schoonman (Eds.), *Solid State Chemistry, Proceedings of the second European Conference Veldhoven, 7–9 June 1982*, Elsevier, Amsterdam, 1983, p. 143.
- [27] V.K. Trunov, Yu.A. Velikodnyi, *Russ. J. Inorg. Chem.* 19 (1974) 1659.
- [28] K. Okada, F. Marumo, S. Iwai, *Acta Crystallogr. B* 33 (1977) 3345.